ChemPhysChem

Research Article
doi.org/10.1002/cphc.202400022

Chemistry Europe
European Chemical Societies Publishing

www.chemphyschem.org

# A Deeper Insight into the Supramolecular Activation of Oxidative Addition Reactions Involving Pincer-Rhodium(I) Complexes

Tiago Vinicius Alves,[a, b] Eduardo Peris,[c] and Israel Fernández*[a]

The factors governing the acceleration of the oxidative addition of methyl iodide to pincer rhodium(I)-complexes induced by coronene have been computationally explored in detail using quantum chemical methods. Both the parent reaction and the coronene-mediated process proceed via a stepwise $S_N2$-type mechanism. It is found that the acceleration of the process derives from the formation of an initial supramolecular complex, mainly stabilized by electrostatic and π-π interactions, which significantly increases the electron richness of the complex. The impact of this effect on the reaction barrier has been quantitatively analyzed by applying the activation strain model in combination with the energy decomposition analysis method. In addition, the influence of other polycyclic aromatic hydrocarbons on the oxidative reaction has been also considered.

## Introduction

The oxidative addition (OA) reaction involving transition-metal complexes is arguably one of the most fundamental processes in organometallic chemistry.[1,2] This transformation typically involves the rupture of an E–X bond (where X is usually a halogen atom) with the concomitant formation of two new bonds within the transition metal (TM), which in turn increases its oxidation state by two units. Due to its ubiquity in a good number of TM-catalysed reactions, this fundamental process has been extensively investigated from both experimental and theoretical points of view.[3] From a mechanistic point of view, the oxidative addition reaction may proceed through two alternative reaction mechanisms, namely a concerted pathway involving the simultaneous formation of the TM–E and TM–X bonds in the corresponding transition state, or an $S_N2$-type mechanism involving a stepwise process with the formation of a cationic intermediate upon nucleophilic addition of the TM to the E–X bond.[3]

Much progress has been made towards the improvement of the OA reaction either by modifying the TM fragment or the E–X substrate. For instance, it is widely accepted that the process is favored when using electron-rich metal centers, that is by using TMs in low oxidation states bound to ligands that are strongly electron-donating.[4] In addition, steric effects and the bite angle of ancillary ligands also influence the rate of the OA reaction.[5] In this regard, some of us recently used a different approach to enhance the reaction rate of the OA reaction. It was found that the process involving the OA of methyl iodide to the pincer-rhodium(I) complex **1** becomes substantially accelerated in the presence of coronene (Scheme 1a).[6] Indeed, a 2.6-fold increase in the reaction rate was observed along with a clear reduction of the activation

[a] Dr. T. Vinicius Alves, Prof. Dr. I. Fernández
Departamento de Química Orgánica and Centro de Innovación en Química Avanzada (ORFEO-CINQA)
Facultad de Ciencias Químicas, Universidad Complutense de Madrid
Ciudad Universidad, 28040-Madrid, Spain
E-mail: israel@quim.ucm.es

[b] Dr. T. Vinicius Alves
Departamento de Físico-Química
Instituto de Química, Universidade Federal da Bahia
Av. Barão de Jeremoabo, 147, 40170-115-Salvador, Bahia, Brazil

[c] Prof. Dr. E. Peris
Institute of Advanced Materials (INAM) and Centro de Innovación en Química Avanzada (ORFEO-CINQA)
Universitat Jaume I
Av. Vicente Sos Baynat s/n, 12071-Castellón, Spain
E-mail: eperis@uji.es

Supporting information for this article is available on the WWW under https://doi.org/10.1002/cphc.202400022



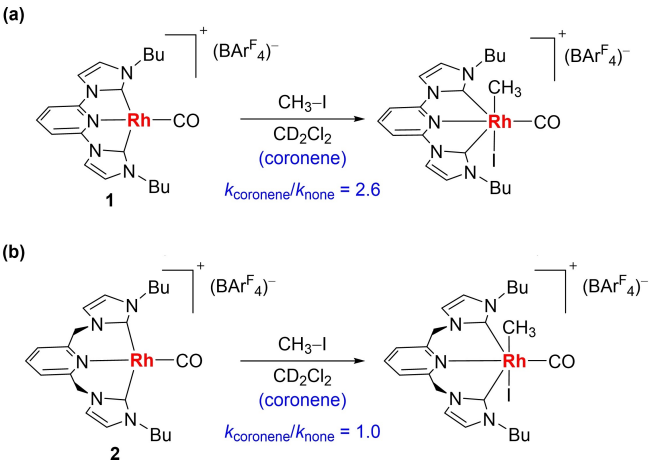


**Scheme 1.** Oxidative addition reactions involving pincer-Rh(I) complexes **1** and **2**.

enthalpy of the process ($\Delta\Delta H^{\neq} = 2.2$ kcal/mol). According to titration and IR experiments, it was suggested that the observed acceleration mainly derives from the formation of a supramolecular complex between the planar π-core of **1** and coronene, which increases the electron richness at the metal fragment thus facilitating the OA reaction. This was supported by the fact that the analogous reaction involving the strongly related non-planar complex **2**, did not exhibit any measurable effect on the reaction rate upon addition of coronene (Scheme 1b). Moreover, this activation strategy has proven to enhance the catalytic efficiency of complex **1** compared to other related pincer-Rh(I) complexes.[6,7]

Despite the above findings, the ultimate physical factors controlling the rate enhancement of the process are not completely understood so far, thus limiting future developments of this activation strategy. Built on these grounds, we decided to investigate computationally the physical factors governing the acceleration of the OA reaction of methyl iodide to the Rh(I) complex **1** in the presence of coronene. To this end, we applied the Activation Strain Model (ASM) of reactivity[8] in combination with the Energy Decomposition Analysis (EDA) method,[9] an approach that has greatly contributed to our current understanding of fundamental transformations in chemistry,[10] and particularly, of oxidative additions mediated by transition metal complexes and related systems.[11] In addition, the influence of the nature of the polycyclic aromatic hydrocarbon (PAH) on the process shall be discussed as well.

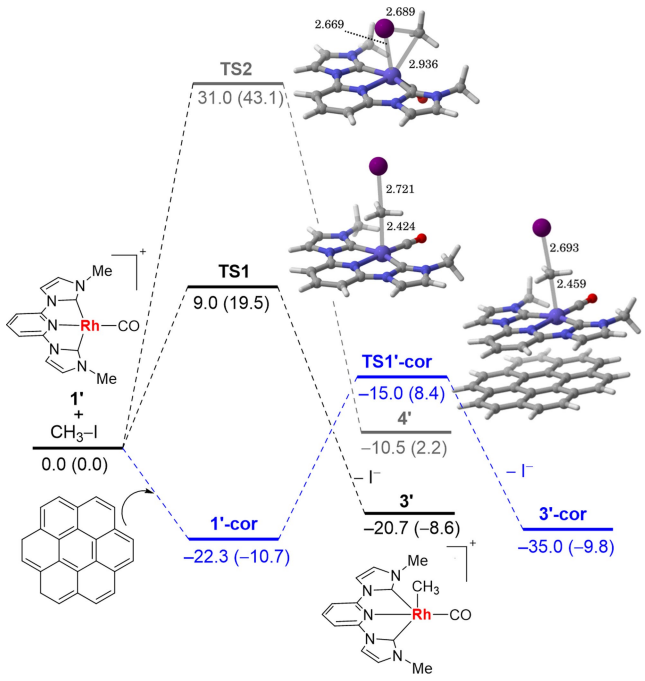


**Figure 1.** Computed reaction profile for the parent reaction between **1'** and methyl iodide and the analogous transformation in the presence of coronene. Plain values refer to the relative electronic energies, including zero-point corrections, whereas values within parentheses refer to relative free energies (ΔG, at 298 K). Energies and bond distances are given in kcal/mol and angstroms, respectively. All data were computed at the PCM($CH_2Cl_2$)-B3LYP-D3/def2-TZVPP//PCM($CH_2Cl_2$)-B3LYP-D3/def2-SVP level.

## Results and Discussion

We first studied the mechanism involved in this particular OA reaction. According to the experimentally measured large negative activation entropy ($\Delta S^{\neq}$ ca. −61 cal/molK),[6] the process is suggested to follow an associative mechanism, which is compatible with a $S_N2$ mechanism, as reported in previous computational and experimental studies on related OA reactions involving Rh(I)-complexes.[12] To further confirm this point, we compared the two possible OA mechanisms for the parent reaction between **1'** (a model system of **1** where the butyl groups were replaced by methyl groups) and $CH_3$–I. From the data displayed in Figure 1, which shows the reaction profiles for both alternative pathways, it becomes clear that the $S_N2$-like mechanism (leading to the dicationic intermediate **3'** via **TS1**) is strongly favored over the concerted pathway (via **TS2**) from both kinetic ($\Delta\Delta G^{\neq} = 23.6$ kcal/mol) and thermodynamic ($\Delta\Delta G = 10.8$ kcal/mol) points of view, in clear agreement with the experimental findings.[6] In addition, we found a large negative activation entropy for the transition state associated with the $S_N2$ mechanism ($\Delta S^{\neq} = -34.2$ cal/molK) whereas a positive value was found for the alternative process involving **TS2** ($\Delta S^{\neq} = +39.9$ cal/molK).

Once the $S_N2$-type route reaction was established as the most plausible pathway for this particular OA reaction, we focused on the influence of the coronene on the transformation. As shown in Figure 1, the process in the presence of coronene begins with the exergonic formation (ΔG = −10.7 kcal/mol) of an initial intermediate **1'-cor** featuring a clear π–π interaction between the molecule of coronene and the Rh(I)-complex. From **1'-cor**, the $S_N2$-oxidative addition takes place through **TS1'-cor** affording the corresponding dicationic intermediate **3'-cor** (an analogous species to **3'** interacting with coronene). According to the computed energies shown in Figure 1, it becomes clear that the addition of coronene renders a much more favored AO reaction than the parent reaction without coronene, all along the entire reaction coordinate. In particular, the computed activation enthalpy difference (at 313 K, i.e. the temperature used in the kinetics experiments) between the parent reaction and the analogous reaction mediated by coronene of $\Delta\Delta H^{\neq} = 1.9$ kcal/mol, is nearly identical to that measured experimentally ($\Delta\Delta H^{\neq} = 2.2$ kcal/mol),[6] and thus justifies the same acceleration of the process. In fact, by applying the Transition State Theory (TST), the computed reaction rate ratio $k_{coronene}/k_{none}$ of 2.8 nearly matches perfectly the experimental one ($k_{coronene}/k_{none} = 2.6$), thus further supporting the accuracy of the selected computational method for this study. Nevertheless, it should be noted that in the calculations complete formation of the supramolecular complex is assumed, while under the experimental conditions, only a ca. 50% of the supramolecular adduct may have been formed according to the measured equilibrium constant ($K = 270 \pm 9\ M^{-1}$).[6]

The structure and bonding situation of the key initial supramolecular complex deserve further analysis. Besides coronene, we also considered other smaller polycyclic aromatic molecules (PAH) such as anthracene and pyrene (also consid-

ered in the experiments),[6] as well as the bowl-shaped corannulene to better understand the interaction between the PAH and the rhodium complex. The π–π interaction between the PAH and the planar π-core of the pincer ligand was clearly confirmed by means of the NCIPlot method,[13] as shown in Figure 2 (greenish surfaces). Interestingly, this π-π interaction does not only involve the π-core of the pincer ligand but also the carbonyl ligand. For this reason, the corresponding ν(CO) stretching frequencies may not univocally correlate with the intrinsic backdonation from the metal, as observed in related carbonyl complexes.[14] From our analysis, it becomes evident

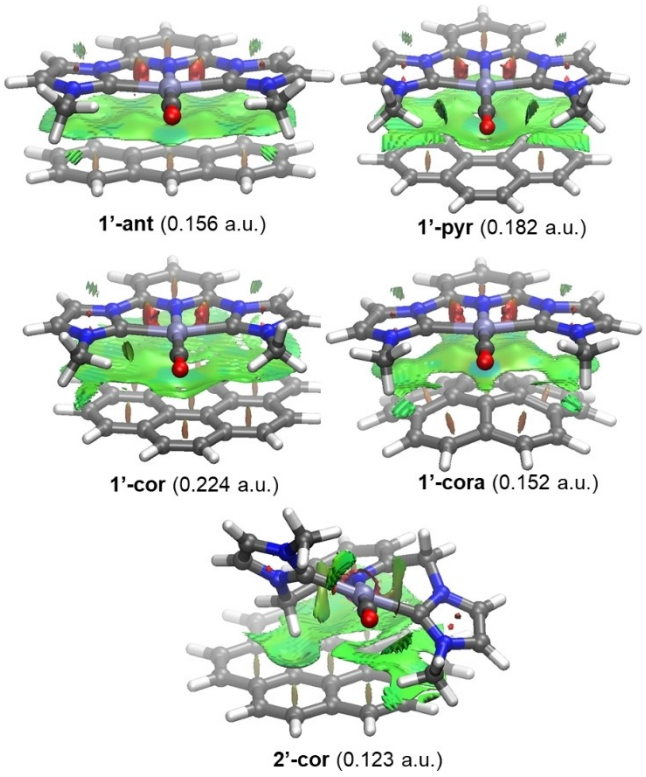


**Figure 2.** Contour plots of the reduced density gradient isosurfaces (density cutoff of 0.04 a.u.) in the initial supramolecular complexes **1'-PHA** (ant = anthracene, pyr = pyrene, cor = coronene and cora = corannulene) and **2'-cor**. The greenish surfaces indicate attractive non-covalent interactions and the numbers correspond to the magnitude of the integration of the real space functions within the reduced density gradient isosurface.

that the stronger interaction between the PAH and **1'** occurs in the **1'-cor** complex (0.224 a.u.), as a consequence of the larger π-surface of coronene when compared to its smaller planar analogs anthracene (0.156 a.u.) and pyrene (0.182 a.u.). Not surprisingly, the smaller available π-surface of the curved corannulene system (**1'-cora**) also results in a weaker π–π interaction (i.e. smaller greenish surface, 0.152 a.u.) as compared to **1'-cor**. The situation is similar in complex **2'** (a model of complex **2** where the butyl groups were replaced again by methyl groups) because its non-planar structure hampers the π-π interaction with coronene leading to a weaker interaction (0.123 a.u., despite the occurrence of CH···π interactions in this particular supramolecular complex). For this reason, no significant acceleration of the oxidative addition reaction was found experimentally in the analogous process involving complex **2** (see above), which is confirmed by the negligible activation barrier difference computed for the process involving **2'** in the absence ($\Delta G^{\neq} = 20.8$ kcal/mol) and presence ($\Delta G^{\neq} = 20.4$ kcal/mol) of coronene.

Further quantitative insight into the interaction between the PAHs and **1'** in the supramolecular complexes can be gained by applying the Energy Decomposition Analysis (EDA).[9] This method was selected because it is particularly useful to quantitatively analyze the nature of non-covalent interactions.[15] From the data in Table 1, it is confirmed that the interaction between the PAH molecule and **1'** becomes stronger as the π-surface of the PAH increases. This is why the π-complex involving coronene, **1'-cor**, which has the largest π-surface and higher electron-richness than pyrene or anthracene, exhibits the strongest interaction ($\Delta E_{int} = -27.5$ kcal/mol) of the entire series. This result is consistent with the much higher binding constant measured experimentally for the association of coronene with **1** ($K = 270 \pm 9\ M^{-1}$) as compared to that involving pyrene ($K = 4.39 \pm 0.01\ M^{-1}$).[6] Not surprisingly, the interaction between **1'** and corannulene is comparatively weaker than that of coronene, and similar to that computed for the pyrene complexes ($\Delta E_{int} \approx -22$ kcal/mol). Strikingly, the strength of the interaction between the PAH and complex **1'**, measured by $\Delta E_{int}$, correlates with the activation barrier of the corresponding OA reaction:[16] $\Delta G^{\neq} = 15.1$ kcal/mol (anthracene) > $\Delta G^{\neq} = 14.1$ kcal/mol (corannulene) > $\Delta G^{\neq} = 12.6$ kcal/mol (pyrene) >

**Table 1.** Energy Decomposition Analysis (energy values in kcal/mol) of the supramolecular complexes **1'-PAH**.[a] All data were computed at the ZORA-B3LYP-D3/TZ2P//PCM($CH_2Cl_2$)-B3LYP-D3/def2-SVP level.

| Complex | $\Delta E_{int}$ | $\Delta E_{Pauli}$ | $\Delta E_{elstat}$[b] | $\Delta E_{orb}$[b] | $\Delta E_{disp}$[b] |
|---|---|---|---|---|---|
| **1'-ant** | −19.2 | 28.6 | −15.8 (33.1%) | −7.8 (16.3%) | −24.2 (50.6%) |
| **1'-pyr** | −22.4 | 31.4 | −17.5 (32.6%) | −8.9 (16.5%) | −27.4 (50.9%) |
| **1'-cor** | −27.5 | 37.1 | −21.1 (32.7%) | −9.3 (14.4%) | −34.2 (52.9%) |
| **1'-cora** | −22.8 | 34.6 | −22.5 (39.2%) | −9.9 (17.2%) | −25.0 (43.6%) |

[a] Using **1'** and the corresponding PAH as fragments. [b] The percentage values in parentheses give the contribution to the total attractive interactions $\Delta E_{elstat} + \Delta E_{orb} + \Delta E_{disp}$.

$\Delta G^{\neq} = 8.4$ kcal/mol (coronene). This finding confirms the critical role of the nature of the PAH in the transformation.

The partitioning of the interaction energy into its different energy contributors indicates that in all cases the bonding between the PAH and the Rh(I)-complex is dominated by a combination of dispersion forces (ca. 52% to the total interaction) and electrostatic interactions (ca. 33%), confirming the non-covalent nature of the interaction. At variance, the orbital interaction is comparatively much weaker and contributes only ca. 15% to the total attractions. Interestingly, the coronene complex **1′-cor** benefits from the strongest attractive terms of the entire series. These favorable interactions not only offset the highest Pauli repulsion computed for this system (as a consequence of the high electron-richness of the coronene) but are also responsible for the strongest $\Delta E_{int}$ value computed for this particular supramolecular complex.

We next analyzed quantitatively the reasons behind the observed acceleration of the OA involving the pincer Rh(I)-complex and methyl iodide in the presence of coronene with the help of the Activation Strain Model (ASM) of reactivity.[8] Figure 3 shows the corresponding activation strain diagrams (ASDs) for the parent reaction involving **1′** + $CH_3I$ (black curves) and the analogous process in the presence of coronene **1′-cor** + $CH_3I$ (red curves), from the early stages of the transformation up to the corresponding transition states and projected onto the Rh···C bond-forming distance. From the data in Figure 3, it becomes evident that the lower barrier computed for the AO reaction occurring in the presence of coronene is not at all due to the $\Delta E_{strain}$ term, which is actually slightly less destabilizing for the parent reaction practically along the entire reaction coordinate. This can be ascribed to the presence of coronone, which makes the distortion of the Rh(I)-complex more difficult. At variance, the process involving **1′-cor** benefits from a stronger interaction between the deformed reactants ($\Delta E_{int}$), particularly at the transition state region. Therefore, it can be concluded that the supramolecular activation of the AO reaction, occurring upon addition of coronene, finds its origin exclusively in a stronger interaction between the reactants along the transformation. Similar ASDs were computed for the related reactions involving the other considered PAHs (see Figure S2 in the Supporting Information).

The origin of the above-mentioned stronger interaction computed for the process involving **1′-cor** can be found by applying the EDA method. Figure 4 graphically shows the evolution of the EDA terms along the reaction coordinate once again from the beginning of the processes up to the corresponding transition states and projected onto the Rh···C bond-forming distance (see Figure S3 for the corresponding EDAs for the process involving the other PAHs). As depicted in Figure 4, the parent reaction benefits from a less stabilizing reaction Pauli repulsion along the entire transformation, which clearly indicates that the electron-richness of the supramolecular complex **1′-cor** is higher than that of the parent complex **1′** as a consequence of the interaction with coronene. This more destabilizing Pauli repulsion computed for the **1′-cor** + $CH_3I$ reaction is nevertheless compensated by both stronger electrostatic and orbital interactions, particularly at the transition state region, as compared to the parent reaction involving **1′** (the contribution from dispersion interactions is nearly identical for both processes). For instance, at the same consistent Rh···C bond-forming distance of 2.5 Å,[17] $\Delta\Delta E_{Pauli} = 2.6$ kcal/mol favoring the process involving **1′**, whereas $\Delta\Delta E_{orb} = 1.7$ kcal/mol and $\Delta\Delta E_{elstat} = 2.4$ kcal/mol favoring the coronene mediated reaction and $\Delta\Delta E_{disp} = 0.4$ kcal/mol. Therefore, the combination of both more stabilizing electrostatic attractions and orbital interactions renders the total interaction between the reactants stronger for the coronene reaction which

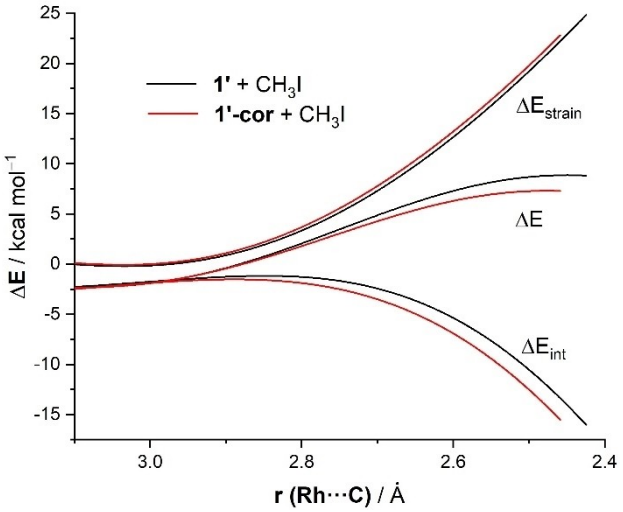


**Figure 3.** Comparative activation strain analyses of the oxidative addition reactions between $CH_3I$ and **1′** (black lines) and coronene complex **1′-cor** (red lines) projected onto the Rh···C bond-forming distance. All data have been computed at the PCM($CH_2Cl_2$)-B3LYP-D3/def2-TZVPP//PCM($CH_2Cl_2$)-B3LYP-D3/def2-SVP level.

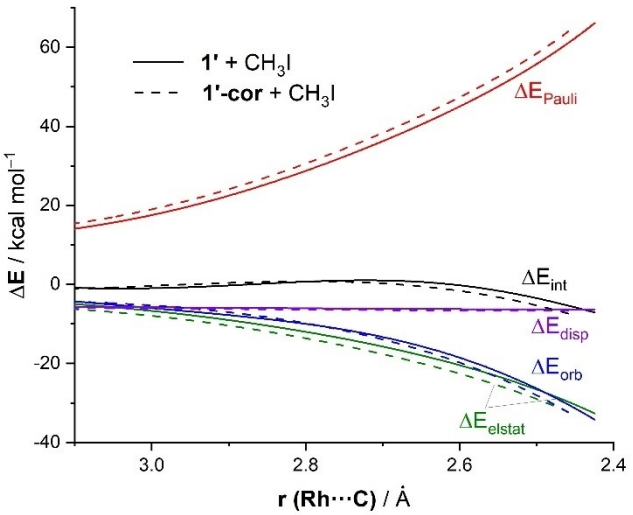


**Figure 4.** Comparative energy decomposition analyses of the oxidative addition reactions between $CH_3I$ and **1′** (solid lines) and coronene complex **1′-cor** (dotted lines) projected onto the Rh···C bond-forming distance. All data have been computed at the ZORA-B3LYP-D3/TZ2P//PCM($CH_2Cl_2$)-B3LYP-D3/def2-SVP level.

ultimately is translated into the lower barrier computed for this process.

The Natural Orbital for Chemical Valence (NOCV)[18] extension of the EDA method was applied next to not only visualize but also quantify the main orbital interactions involved in these OA reactions. This approach indicates that the reaction is mainly dominated by the charge flow from a doubly occupied d-atomic orbital of rhodium to the σ*(C–I) of methyl iodide (Figure 5). Interestingly, according to the associated stabilizing energies (ΔE(ρ1)), this d(Rh)→σ*(C–I) orbital interaction is stronger for the process mediated by coronene as compared to the parent reaction (see values computed at the same consistent Rh···C bond-forming distance of 2.46 Å), which is translated into the stronger total orbital interactions computed for the **1'-cor** + $CH_3I$ reaction commented above.

In addition, the NOCV method also shows that the total electronic charge transferred from the d-atomic orbital of rhodium to the σ*(C–I) molecular orbital is markedly higher for the process involving **1'-cor** (0.63e vs 0.58e, at the same consistent Rh···C distance),[16] which is mainly responsible for the stronger electrostatic attractions between the reactants. Results above therefore indicate that the PHA induces a significant increase in the electron-richness of the Rh(I)-complex which is translated into stronger electrostatic and orbital interactions with methyl iodide and ultimately, into the observed acceleration of the OA reaction.

## Conclusions

From the computational study reported herein, the following conclusions can be drawn: (1) the oxidative addition reaction of methyl iodide to pincer-Rh(I) complexes proceeds via a stepwise $S_N2$-mechanism which is both kinetically and thermodynamically favored over the alternative concerted mechanism. (2) This process can be significantly accelerated upon the addition of a polycyclic aromatic hydrocarbon, in particular, coronene. (3) This is due to the formation of an initial supramolecular complex between the PAH and the Rh(I)-compound, which is mainly stabilized by non-covalent electrostatic and dispersion (π–π) interactions. (4) The nature of the PAH dramatically influences its interaction with the Rh(I)-complex in such a way that PAH molecules with larger available π-surfaces lead to stronger interactions. (5) This supramolecular interaction increases the electron-richness of the Rh(I)-species leading to a stronger interaction with methyl iodide, which, in turn, derives from stronger electrostatic attractions together with more stabilizing orbital interactions, mainly involving the d(Rh)→σ*-(C–I) orbital interaction. In summary, the results presented herein not only support the previously suggested supramolecular activation of the process but also rationalize, in a quantitative manner, the reasons behind the observed acceleration of the OA reaction. Further work is underway to confirm the generality of this activation mode to related transition metal pincer-type complexes.

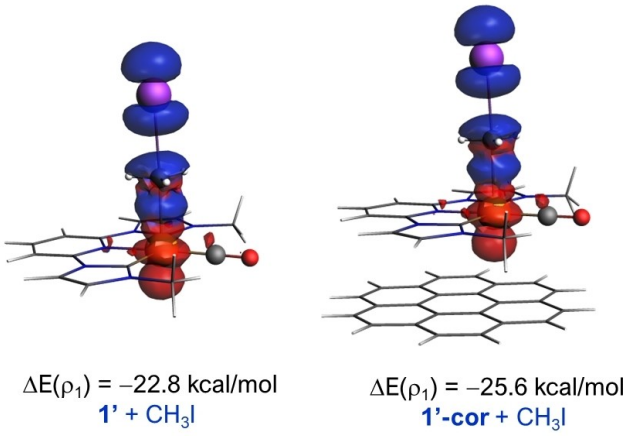


**Figure 5.** Contour plots of the NOCV deformation densities ρ (isosurface value of 0.001 a.u.) and the associated energies ΔE(ρ) for the main orbital interaction present at the initial oxidative addition reaction involving methyl iodide and **1'** (left) and **1'-cor** (right). The electronic charge flows from red to blue. All data have been computed at the ZORA-B3LYP-D3/TZ2P//PCM($CH_2Cl_2$)-B3LYP-D3/def2-SVP level.

## Supporting Information

Figures S1–S3 and Cartesian coordinates and energies of all species discussed in the text.

## Computational Details

Geometry optimizations of the molecules were performed without symmetry constraints using the Gaussian09 (RevD.01) suite of programs[19] at the dispersion-corrected B3LYP[20]-D3[21]/def2-SVP[22] level (which includes the corresponding pseudopotentials for rhodium and iodine atoms) including solvent effects (solvent = dichloromethane) with the Polarization Continuum Model (PCM) method.[23] Reactants and adducts were characterized by frequency calculations and have positive definite Hessian matrices. Transition states show only one negative eigenvalue in their diagonalized force constant matrices, and their associated eigenvectors were confirmed to correspond to the motion along the reaction coordinate under consideration using the Intrinsic Reaction Coordinate (IRC) method.[24] Energy refinements were carried out by means of single-point calculations at the same DFT level using the much larger triple-ζ basis set def2-TZVPP.[22] This level is denoted PCM($CH_2Cl_2$)-B3LYP-D3/def2-TZVPP//PCM($CH_2Cl_2$)-B3LYP-D3/def2-SVP.

### Activation Strain Model of Reactivity and Energy Decomposition Analysis

Within the ASM method,[8] also known as the distortion/interaction model,[8c] the potential energy surface ΔE(ζ) is decomposed along the reaction coordinate, ζ, into two contributions, namely the strain $\Delta E_{strain}(\zeta)$ associated with the deformation (or distortion) required by the individual reactants during the process and the interaction $\Delta E_{int}(\zeta)$ between these increasingly deformed reactants:

$$\Delta E(\zeta) = \Delta E_{strain}(\zeta) + \Delta E_{int}(\zeta)$$

Within the EDA method,[9] the interaction energy can be further decomposed into the following chemically meaningful terms:

$$\Delta E_{int}(\zeta) = \Delta E_{Pauli}(\zeta) + \Delta E_{elstat}(\zeta) + \Delta E_{orb}(\zeta) + \Delta E_{disp}(\zeta)$$

The term $\Delta V_{elstat}$ corresponds to the classical electrostatic interaction between the unperturbed charge distributions of the deformed reactants and is usually attractive. The Pauli repulsion $\Delta E_{Pauli}$ comprises the destabilizing interactions between occupied orbitals and is responsible for any steric repulsion. The orbital interaction $\Delta E_{orb}$ accounts for bond pair formation, charge transfer (interaction between occupied orbitals on one moiety with unoccupied orbitals on the other, including HOMO-LUMO interactions), and polarization (empty-occupied orbital mixing on one fragment due to the presence of another fragment). Moreover, the NOCV (Natural Orbital for Chemical Valence)[18] extension of the EDA method has been also used to further partition the $\Delta E_{orb}$ term. The EDA-NOCV approach provides pairwise energy contributions for each pair of interacting orbitals to the total bond energy.

The program package ADF[25] was used for EDA calculations using the optimized PCM($CH_2Cl_2$)-B3LYP-D3/def2-SVP geometries at the same B3LYP-D3 level in conjunction with a triple-ζ-quality basis set using uncontracted Slater-type orbitals (STOs) augmented by two sets of polarization functions with a frozen-core approximation for the core electrons.[26] Auxiliary sets of s, p, d, f, and g STOs were used to fit the molecular densities and to represent the Coulomb and exchange potentials accurately in each SCF cycle.[27] Scalar relativistic effects were incorporated by applying the zeroth-order regular approximation (ZORA).[28] This level of theory is denoted ZORA-B3LYP-D3/TZ2P//PCM($CH_2Cl_2$)-B3LYP-D3/def2-SVP.

## Acknowledgements

This work was supported by the Spanish MCIN/AEI/10.13039/501100011033 (Grants PID2019-106184GB-I00 and PID2022-139318NB-I00 to I. F. and PID2021-127862NB-I00 and RED2022-134287-T to E.P.). T. V. A. acknowledges the Coordenação de Aperfeiçoamento de Pessoal de Nível Superior – Brazil (CAPES) for the visiting professor scholarship (CAPES-PrInt – 88887.803486/2023–00).

## Conflict of Interests

The authors declare no conflict of interest.

## Data Availability Statement

The data that support the findings of this study are available in the supplementary material of this article.

**Keywords:** oxidative addition · rhodium · polycyclic aromatic hydrocarbon · reactivity · bonding

[1] a) R. H. Crabtree, *The Organometallic Chemistry of the Transition Metals*, 3rd ed., Wiley, New York, **2001**; b) C. Elschenbroich, *Organometallics*, 3rd ed., Wiley-VCH, Weinheim, **2006**.
[2] a) V. V. Grushin, H. Alper, *Chem. Rev.* **1994**, *94*, 1047–1062; b) C. Amatore, A. Jutand, *Acc. Chem. Res.* **2000**, *33*, 314–321; c) T.-Y. Luh, M.-K. Leung, K. T. Wong, *Chem. Rev.* **2000**, *100*, 3187–3204.
[3] For selected reviews on computational studies, see: a) M. García-Melchor, A. A. C. Braga, A. Lledós, G. Ujaque, F. Maseras, *Acc. Chem. Res.* **2013**, *46*, 2626–2634; b) T. Sperger, I. A. Sanhueza, I. Kalvet, F. Schoenebeck, *Chem. Rev.* **2015**, *115*, 9532–9586.
[4] a) M. D. Su, S. Y. Chu, *J. Phys. Chem. A* **1997**, *101*, 6798–6806; b) M. D. Su, S. Y. Chu, *Inorg. Chem.* **1998**, *37*, 3400–3406; c) K. Krogh-Jespersen, M. Czerw, K. M. Zhu, B. Singh, M. Kanzelberger, N. Darji, P. D. Achord, K. B. Renkema, A. S. Goldman, *J. Am. Chem. Soc.* **2002**, *124*, 10797–10809; d) R. Fazaeli, A. Ariafard, S. Jamshidi, E. S. Tabatabaie, K. A. Pishro, *J. Organomet. Chem.* **2007**, *692*, 3984–3993; e) D. Y. Wang, Y. Choliy, M. C. Haibach, J. F. Hartwig, K. Krogh-Jespersen, A. S. Goldman, *J. Am. Chem. Soc.* **2016**, *138*, 149–163.
[5] a) P. Dierkes, P. van Leeuwen, *J. Chem. Soc. Dalton Trans.* **1999**, 1519–1529; b) S. Gu, R. J. Nielsen, K. H. Taylor, G. C. Fortman, J. Chen, D. A. Dickie, W. A. Goddard, III, T. B. Gunnoe, *Organometallics* **2020**, *39*, 1917–1933; c) P. van Leeuwen, P. C. J. Kamer, J. N. H. Reek, P. Dierkes, *Chem. Rev.* **2000**, *100*, 2741–2769; d) Z. Freixa, P. van Leeuwen, *Dalton Trans.* **2003**, 1890–1901; e) C. M. Frech, D. Milstein, *J.Am. Chem. Soc.* **2006**, *128*, 12434–12435; f) M. N. Birkholz, Z. Freixa, P. van Leeuwen, *Chem. Soc. Rev.* **2009**, *38*, 1099–1118.
[6] S. Martínez-Vivas, M. Poyatos, E. Peris, *Angew. Chem. Int. Ed.* **2023**, *62*, e202307198.
[7] S. Martínez-Vivas, D. G. Gusev, M. Poyatos, E. Peris, *Angew. Chem. Int. Ed.* **2023**, *62*, e202313899.
[8] a) I. Fernández, F. M. Bickelhaupt, *Chem. Soc. Rev.* **2014**, *43*, 4953–4967; b) L. P. Wolters, F. M. Bickelhaupt, *WIREs Comput. Mol. Sci.* **2015**, *5*, 324–343; c) F. M. Bickelhaupt, K. N. Houk, *Angew. Chem. Int. Ed.* **2017**, *56*,10070–10086. See also; d) I. Fernández, in *Discovering the Future of Molecular Sciences* (Ed.: B.Pignataro), Wiley-VCH, Weinheim, **2014**, pp. 165–187.
[9] For reviews on the EDA method, see: a) F. M. Bickelhaupt, E. J. Baerends, in *Reviews in Computational Chemistry*, (Eds. K. B. Lipkowitz, D. B. Boyd), Wiley-VCH: New York, **2000**, Vol. 15, pp. 1–86; b) M. von Hopffgarten, G. Frenking, *WIREs Comput. Mol. Sci.* **2012**, *2*, 43–62; c) I. Fernández, in *Applied Theoretical Organic Chemistry*, (Ed. D. J. Tantillo), World Scientific, New Jersey, **2018**, pp. 191–226.
[10] Selected recent representative examples: a) D. N. Kamber, S. S. Nguyen, F. Liu, J. S. Briggs, H.-W. Shih, R. D. Row, Z. G. Long, K. N. Houk, Y. Liang, J. A. Prescher, *Chem. Sci.* **2019**, *10*, 9109–9114; b) A. Couce-Ríos, A. Lledós, I. Fernández, G. Ujaque, *ACS Catal.* **2019**, *9*, 848–858; c) I. Fernández, *Chem. Sci.* **2020**, *11*, 3769–3779; d) P. Vermeeren, T. A. Hamlin, I. Fernández, F. M. Bickelhaupt, *Chem. Sci.* **2020**, *11*, 8105–8112; e) T. A. Hamlin, F. M. Bickelhaupt, I. Fernández, *Acc. Chem. Res.* **2021**, *54*, 1972–1981; f) T. Hansen, P. Vermeeren, F. M. Bickelhaupt, T. A. Hamlin, *Angew. Chem. Int. Ed.* **2021**, *60*, 20840–20848; g) T. A. Hamlin, F. M. Bickelhaupt, I. Fernández, *Acc. Chem. Res.* **2021**, *54*, 1972–1981; h) I. Fernández, *Chem. Commun.* **2022**, *58*, 4931–4940.
[11] a) G. T. de Jong, F. M. Bickelhaupt, *J. Chem. Theory Comput.* **2007**, *3*, 514–529; b) G. T. de Jong, F. M. Bickelhaupt, *ChemPhysChem.* **2007**, *8*, 1170–1181; c) I. Fernández, L. P. Wolters, F. M. Bickelhaupt, *J. Comput. Chem.* **2014**, *35*, 2140–2145; d) Y. García-Rodeja, F. M. Bickelhaupt, I. Fernández, *Chem. Eur. J.* **2016**, *22*, 13669–13676. See also, reference [8b].
[12] a) H. C. Martin, N. H. James, J. Aitken, J. A. Gaunt, H. Adams, A. Haynes, *Organometallics* **2003**, *22*, 4451–4458; b) J. A. Gaunt, V. C. Gibson, A. Haynes, S. K. Spitzmesser, A. J. P. White, D. J. Williams, *Organometallics* **2004**, *23*, 1015–1023; c) J. M. Wilson, G. J. Sunley, H. Adams, A. Haynes, *J. Organomet. Chem.* **2005**, *690*, 6089–6095; d) M. Feliz, Z. Freixa, P. W. N. M. van Leeuwen, C. Bo, *Organometallics* **2005**, *24*, 5718–5723.
[13] E. R. Johnson, S. Keinan, P. Mori-Sanchez, J. Contreras-García, A. J. Cohen, W. Yang, *J. Am. Chem. Soc.* **2010**, *132*, 6498–6506.
[14] D. A. Valyaev, R. Brousses, N. Lugan, I. Fernández, M. A. Sierra, *Chem. Eur. J.* **2011**, *17*, 6602–6605.
[15] See, for instance: a) P. R. Horn, Y. Mao, M. Head-Gordon, *Phys. Chem. Chem. Phys.* **2016**, *18*, 23067–23079; b) T. A. Hamlin, I. Fernández, F. M. Bickelhaupt, *Angew. Chem. Int. Ed.* **2019**, *58*, 8922–8926; c) M. Bursch, L. Kunze, A. M. Vibhute, A. Hansen, K. M. Sureshan, P. G. Jones, S. Grimme, D. B. Werz, *Chem. Eur. J.* **2021**, *8*, 4627–4639; d) S. Portela, I. Fernández, *Tetrahedron Chem.* **2022**, *1*, 100008; e) L. de Azevedo Santos, T. C. Ramalho, T. A. Hamlin, F. M. Bickelhaupt, *Chem. Eur. J.* **2023**, *29*, e202203791.
[16] Activation barriers were computed as $\Delta G^{\neq} = G(\mathbf{TS}) - G(\mathbf{1'}) - G(CH_3I) - G\text{-}G(PAH)$. See also Figure S1 in the Supporting Information.
[17] Performing this analysis at a consistent point along the reaction coordinate (near all transition structures), rather than the transition state alone, ensures that the results are not skewed by the position of the transition state.

[18] M. P. Mitoraj, A. Michalak, T. Ziegler, *J. Chem. Theory Comput.* **2009**, *5*, 962–975.
[19] Gaussian 09, Revision D.01, M. J. Frisch, G. W. Trucks, H. B. Schlegel, G. E. Scuseria, M. A. Robb, J. R. Cheeseman, G. Scalmani, V. Barone, G. A. Petersson, H. Nakatsuji, X. Li, M. Caricato, A. Marenich, J. Bloino, B. G. Janesko, R. Gomperts, B. Mennucci, H. P. Hratchian, J. V. Ortiz, A. F. Izmaylov, J. L. Sonnenberg, D. Williams-Young, F. Ding, F. Lipparini, F. Egidi, J. Goings, B. Peng, A. Petrone, T. Henderson, D. Ranasinghe, V. G. Zakrzewski, J. Gao, N. Rega, G. Zheng, W. Liang, M. Hada, M. Ehara, K. Toyota, R. Fukuda, J. Hasegawa, M. Ishida, T. Nakajima, Y. Honda, O. Kitao, H. Nakai, T. Vreven, K. Throssell, J. A. Montgomery, Jr., J. E. Peralta, F. Ogliaro, M. Bearpark, J. J. Heyd, E. Brothers, K. N. Kudin, V. N. Staroverov, T. Keith, R. Kobayashi, J. Normand, K. Raghavachari, A. Rendell, J. C. Burant, S. S. Iyengar, J. Tomasi, M. Cossi, J. M. Millam, M. Klene, C. Adamo, R. Cammi, J. W. Ochterski, R. L. Martin, K. Morokuma, O. Farkas, J. B. Foresman, D. J. Fox, Gaussian, Inc., Wallingford CT, 2016.
[20] a) A. D. Becke, *J. Chem. Phys.* **1993**, *98*, 5648–5652; b) C. Lee, W. Yang, R. G. Parr, *Phys. Rev. B* **1998**, *37*, 785–789; c) S. H. Vosko, L. Wilk, M. Nusair, *Can. J. Phys.* **1980**, *58*, 1200–1211.
[21] S. Grimme, J. Antony, S. Ehrlich, H. Krieg, *J. Chem. Phys.* **2010**, *132*, 154104–19.
[22] F. Weigend, R. Ahlrichs, *Phys. Chem. Chem. Phys.* **2005**, *7*, 3297–3305.
[23] a) S. Miertuš, E. Scrocco, J. Tomasi, *Chem. Phys.* **1981**, *55*, 117–129; b) J. L. Pascual-Ahuir, E. Silla, I. Tuñón, *J. Comput. Chem.* **1994**, *15*, 1127–1138; c) V. Barone, M. Cossi, *J. Phys. Chem. A* **1998**, *102*, 1995–2001.
[24] C. Gonzalez, H. B. Schlegel, *J. Phys. Chem.* **1990**, *94*, 5523–5527.
[25] a) G. te Velde, F. M. Bickelhaupt, E. J. Baerends, C. Fonseca Guerra, S. J. A. van Gisbergen, J. G. Snijders, T. Ziegler, *J. Comput. Chem.* **2001**, *22*, 931–967; b) *ADF2020*, SCM, Theoretical Chemistry, Vrije Universiteit, Amsterdam, The Netherlands, http://www.scm.com.
[26] J. G. Snijders, P. Vernooijs, E. J. Baerends, *At. Data Nucl. Data Tables* **1981**, *26*, 483–509.
[27] J. Krijn, E. J. Baerends, *Fit Functions in the HFS-Method*, Internal Report (in Dutch), Vrije Universiteit Amsterdam, The Netherlands, 1984.
[28] a) E. van Lenthe, E. J. Baerends, J. G. Snijders, *J. Chem. Phys.* **1993**, *99*, 4597–4610; b) E. van Lenthe, E. J. Baerends, J. G. Snijders, *J. Chem. Phys.* **1994**, *101*, 9783–9792; c) E. van Lenthe, A. Ehlers, E. J. Baerends, *J. Chem. Phys.* **1999**, *110*, 8943–8953.

Manuscript received: January 16, 2024
Accepted manuscript online: January 25, 2024
Version of record online: February 8, 2024